CLOUD-RADIATION DIAGNOSTICS USING ERBE AND ISCCP DATA

Jean-Jacques Morcrette

European Centre for Medium range Weather Forecasts
Shinfield Park, Reading, U.K.

Abstract

In an attempt to validate the ECMWF model's cloud and radiation parameterizations, model outputs are processed to reproduce the satellite measurements as closely as possible (the "model-to-satellite" approach). Total radiances (as in ERBE data) and brightness temperatures in the longwave window channel of METEOSAT (as in ISCCP/B3 data) are simulated from cloudiness, temperature and humidity fields derived from the conventional meteorological observations or from the model analyses and forecasts. They are then compared with the equivalent satellite-measured quantities (ISCCP B3 observations over a 5 days period in July 1983; ERBE S8 radiances and fluxes in April 1985).

The good agreement between computed and observed clear-sky radiation allows to use the radiation scheme for computing the clear-sky radiative fluxes required in the cloud radiative forcing approach proposed by Ramanathan (1987).

Whereas the cloud cover diagnosed by the model appears in fair agreement with the observed one, the instantaneous model cloud longwave forcing is underestimated compared with the observed one. This deficiency is related to the underestimation of the diagnosed cloud liquid water content in the model.

The diurnal cycles of surface temperature and cloudiness, over some limited 10 x 10 deg^2 areas, representative of different cloud regimes, are studied using evolution histograms of the brightness temperature. Comparisons of observed and simulated histograms over these areas, allow to pinpoint various other deficiencies in the parameterization of the surface-cloud-radiation interactions.

1. COMPARISON OF MODEL RADIATION FIELDS WITH ERBE OBSERVATIONS

One approach to validate the cloud-radiation parameterization of a GCM is to test its ability to reproduce the first and higher order statistics of the key climate variables driving the general circulation of the earth atmosphere system. Earth radiation budget measurements from satellites, which are uniquely defined and available on different time scales and space resolutions over the whole globe, constitute one of the best tools to help validate the parameterization of the shortwave and longwave radiative transfer processes and to improve generation schemes for the cloud cover in GCM's.

However, whereas the validation in clear-sky atmospheres through such comparisons between observed and computed radiation fields appears quite straightforward, the verification of the impact of cloudiness on the radiation fields is fraught with problems because of the need to know the cloud amount and optical properties, which are notoriously difficult quantities to determine accurately from observations. Actually, radiative fields, either derived from satellite measurements or simulated by model calculations, depend on so many parameters and include so many uncertainties that comparisons, such as those of Morcrette and Geleyn (1985), "fail to provide information on whether discrepancies (or even agreement) are due to inadequate simulations of synoptic structures, poor estimates of the clouds associated with these structures, improper radiation associated with those clouds, or a combination of all of these" (Research Plan for FIRE, 1983).

A simple analysis avoiding this dreadful problem was recently proposed by V. Ramanathan (Hartmann et al., 1986; Ramanathan, 1987). For a region in which there is partial cloud cover, the effect of clouds on some area-mean radiative flux is simply taken to be the difference between that flux and its value for clear skies. The sign of that difference (called cloud radiative forcing) is changed so that implied heating appears as a positive quantity. Further incentive in studying the cloud radiative forcing can be found in some recent experiments with the NCAR Community Climate Model by Slingo and Slingo (1988) which have shown that cloud longwave radiation forcing may be as important as latent heat release in determining the response of the atmosphere to various anomalies, in particular sea surface temperature anomalies.

The recent availability of the first data from the Earth Radiation Budget Experiment (E.R.B.E.) (Barkström, 1984; Barkström and Smith, 1986), that have both a good temporal and spatial resolution, and a high radiometric quality,

makes this cloud radiative forcing analysis particularly attractive. Those measurements provide total longwave and shortwave fluxes, which eliminates the errors linked to the conversion of a narrow-band channel radiance to a broad-band flux. The cloud radiative forcing approach requires the knowledge of the clear-sky fluxes under any circumstances, clear-sky, partly cloudy or overcast. These clear-sky fluxes can be either observed provided the observation period is long enough to ensure a complete geographical coverage of the area of interest, or they can be computed with the help of a radiation scheme from the temperature and humidity profiles, provided that this tool has been first carefully validated.

In the context of the validation of a NWP model, we are more interested in the instantaneous or short time scale radiative impact of cloudiness and its interaction with other physical processes, so that only the approach using computed clear-sky fluxes is relevant. The next two sections are then devoted to assessing the performance of a radiation scheme to compute these clear-sky longwave fluxes. Then we will compare the ECMWF model cloud longwave forcing to the one derived from the ERBE data.

1.1. Comparisons of observed and computed clear-sky longwave radiances

This study was carried out using the cloud-radiation package developed at the University of Lille instead of the operational ECMWF cloud-radiation package for two reasons: first, the ECMWF scheme is designed to calculate fluxes; thus it would not have been possible to perform the first step of the comparisons, namely that of observed vs. computed radiances; second, large systematic errors have been recently found in the operational radiation scheme used at the time of this study (Morcrette, 1989), in both the clear-sky and the cloudy fluxes, so that the present exercise would have been almost useless; third, the radiation package used in this study has since become the operational ECMWF radiation code. The wide-band longwave model used divides the longwave spectrum into 6 intervals in which absorption by H_2O, CO_2 and O_3 are taken into account. Effect of the water continuum absorption is considered in the 350-1250 cm^{-1} region. The pressure and temperature dependence of the absorption in all spectral intervals is taken into account following Morcrette et al. (1986). Different cloud and/or surface radiative properties may be prescribed in the six spectral intervals. Radiance calculations have been performed with an emissivity of 0.95 in the 800-1250 cm^{-1} region, of 1 elsewhere, whereas flux calculations were carried

out with an emissivity of 0.995 in all spectral intervals. Total radiances were calculated using the actual satellite viewing angle, fluxes were evaluated using the so-called diffusivity factor (=1.66) to approximate the angular integration.

To perform these comparisons, we first created a data set including radiosonde (TEMP) and surface (SYNOP) observations at 00 and 12 GMT together with ERBE radiances measurements collocated in both space and time. We kept all ERBE scanner measurements within 1 hour of the time of the observations and within a distance of 120 km from the radiosonde locations. Then a number of criteria were applied to that data set to extract clear-sky atmospheres on which comparisons were actually carried out. We kept only those situations when:

- there is at least one surface observation for the considered radiosounding;
- there are more than 10 ERBE measurements in the 120 km zone around the radiosounding (this eliminates observations under very high viewing angles);
- the radiosounding gives temperature and dew point temperature profiles up to at least 100 hPa and 300 hPa, respectively;
- Three "cloudiness indices" are then defined:
  - i - the cloud fraction reported in the surface observation,
  - ii - the cloud fraction over the considered area estimated by averaging the individual ERBE scene identification index, with the following weights, 0 percent for a "clear-sky scene ID", 33 percent for a "partly cloudy scene ID", 66 percent for a "mostly cloudy scene ID", and 100 percent for an "overcast scene ID",
  - iii- the cloud fraction diagnosed from the temperature and humidity profiles using the operational ECMWF cloud scheme (Slingo, 1987);

  Are only kept as clear-sky atmospheres these situations where these three cloudiness indices give a consistent cloud fraction below 12 percent (1 octa).
- the spatial variance of the radiance field is lower than 5 percent of the mean observed radiance.

Out of about 1500 radiosonde observations generally available at 00 and 12 GMT these criteria stringently restrict the number of usable match-ups to about 10 daily. For those atmospheric profiles then retained, all radiances defined as clear-sky by the ERBE scene ID have been entered into our comparisons. For a given radiosounding, the observed clear-sky radiances

differ from one another because of variations in the satellite viewing angle, of spatial variability of the surface properties (temperature, emissivity) and of the tridimensional distribution of temperature and humidity. Simulated outgoing radiances at the top of the atmosphere are computed for the same distribution of viewing angles but from only one surface temperature and emissivity, and one temperature and humidity profile. The surface temperature is taken from the closest synoptic observation to the radiosounding. Humidity near the surface is derived from the temperature and dew point temperature at 2 m. Temperature and humidity profiles above the highest radiosonde level are derived from climatology. Ozone profile for each radiosonde location is taken from the operational ECMWF ozone climatology. Concentration of carbon dioxide is 340 ppmv.

Figure 1 presents the results of 769 comparisons between calculated and observed clear-sky longwave radiances, corresponding to 122 different radiosoundings selected with the above criteria over the period 15-25 April 1985. The agreement is quite satisfying: the mean bias is 1.9 $W.m^{-2}.sr^{-1}$, the correlation coefficient is 0.93, and 85 percent of the observed variance is simulated by the radiation code. This last result was expected due to the fact that only angular variations were actually simulated. The mean bias varies with the surface type: 3.1 $W\ m^{-2}\ sr^{-1}$ over the ocean, 0.6 $W\ m^{-2}\ sr^{-1}$ over land, 1.3 $W\ m^{-2}\ sr^{-1}$ over snow, and 1.3 $W\ m^{-2}\ sr^{-1}$ over desert areas. Agreement is somewhat better over land and desert because of the 0.95 emssivity that we have assumed in the window region, which is more adapted to land than to water surfaces. For water and snow surfaces, an emissivity closer to unity would give even larger bias, by about 1 $W\ m^{-2}\ sr^{-1}$. This indicates that the definition of the surface temperature is particularly important for such comparisons. The emissivity of ocean water is better known than that of land surfaces which varies between 0.8 and 1 depending on the soil type and its water content. On the other hand, very few measurements of sea surface temperature are available in the SYNOP observations and most of radiosoundings are over land.

The calculated radiances are, on average, larger than the observed ones. The radiation code used for this study does not account for the absorption by methane and nitrous oxide. Calculations with a more detailed narrow-band model of the longwave radiation transfer (Morcrette and Fouquart, 1985) have shown that the effect of these two gases is a decrease of the outgoing radiance by about 1 percent. Uncertainties in the temperature and dew point temperature profiles have also to be taken into account. By and large,

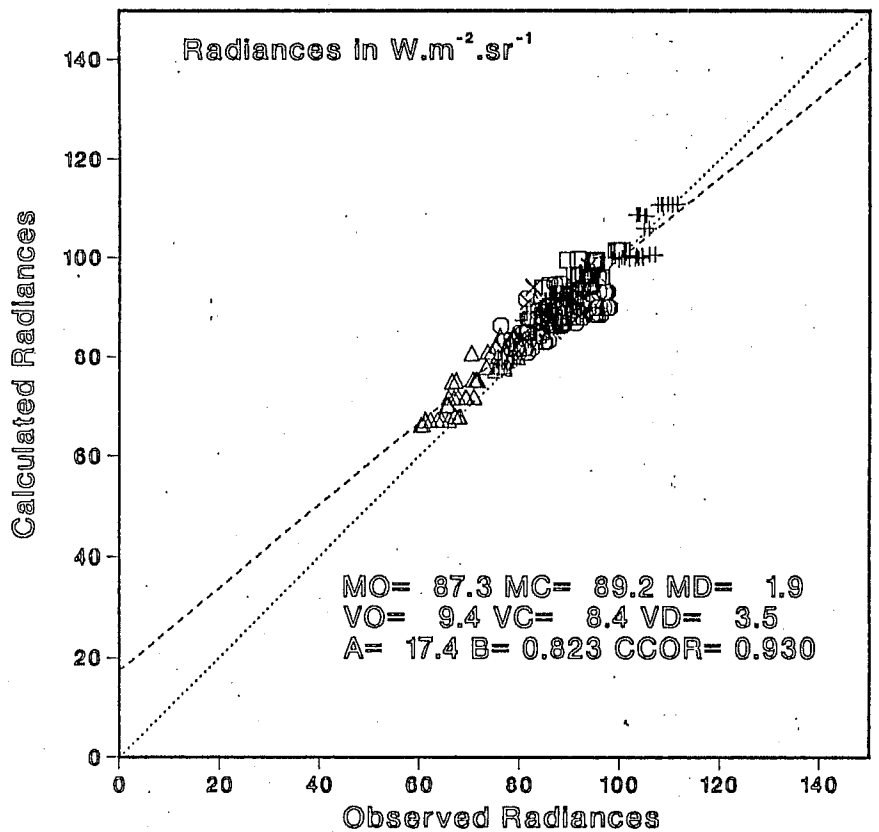

Figure 1: Comparison of calculated and observed clear-sky longwave radiances for a set of 769 radiances corresponding to 122 radiosoundings. is over ocean, over land, over snow, over desert, over coastal regions. MO is the mean value of the observations, MC the value of the computations, MD the mean difference, VO the variance of the observations, VC the variance of the computations, VD the variance of the differences. Dotted is the line of slope 1, dash is the regression line Y = B X + A with a correlation coefficient CCOR.

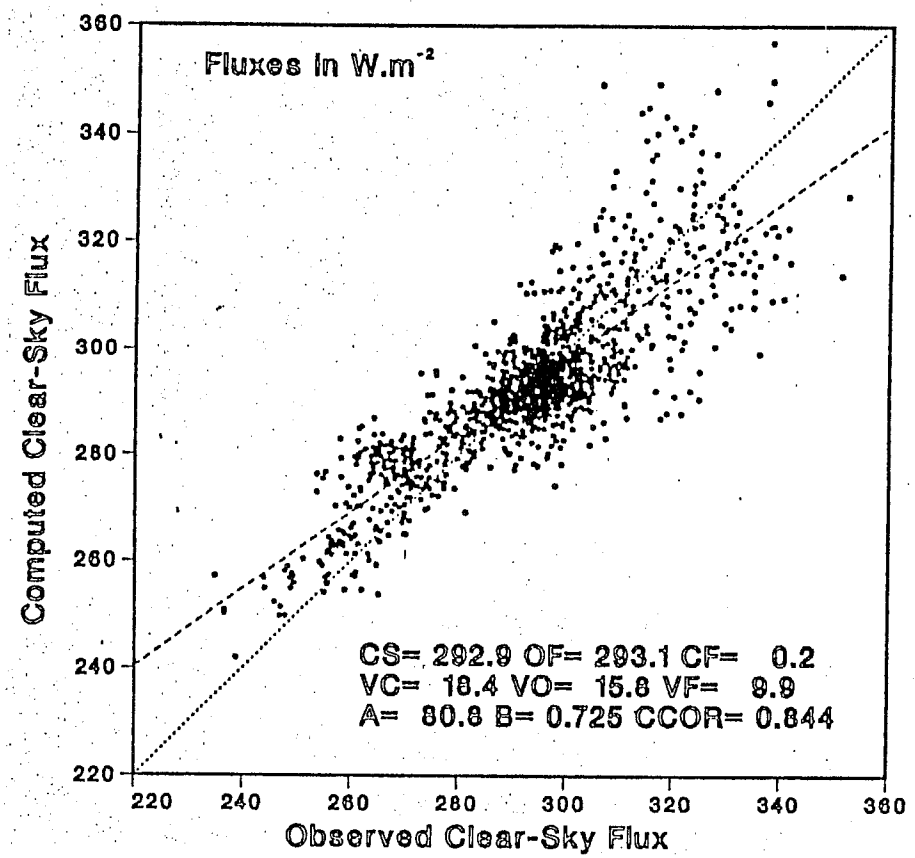

Figure 2: Comparison between calculated and observed clear-sky longwave fluxes. Calculations are performed using the analyzed profiles of T and q for all the T106 model grid boxes which are clear-sky according to the ERBE scene identification index.

comparisons do not show any particular dependence of the bias on the secant of the viewing angle, or on the total amount of water vapour. Thus, the radiation code should give good estimates of the clear-sky outgoing longwave fluxes over various atmospheric situations.

1.2. Comparisons of observed and calculated clear-sky longwave fluxes

Clear-sky outgoing longwave fluxes at the top of the atmosphere have been computed with the same radiation code using the so-called diffusivity factor to approximate the angular integration. Instead of collocated surface and radiosonde observations, the inputs for the radiation code are now the temperature and humidity profiles provided by the ECMWF model for all the T106 grid boxes containing only clear-sky ERBE pixels within 6 hours of a given time. This allows to extend our data set by considering a much larger number of oceanic situations where radiosoundings are few. All calculations have been carried out with the model surface temperature and a 0.995 surface emissivity over the whole longwave spectrum, whatever the surface type is, consistent with the operational ECMWF model value.

Figure 2 presents the results of 2409 comparisons of clear-sky outgoing longwave fluxes for 85/04/21 12GMT. Satellite observations have been kept within 6 hours of that time, whereas simulations correspond to analyzed T and q profiles. The mean bias over the 2409 comparisons of calculated vs. observed clear-sky longwave fluxes is 0.2 W m^{-2}.

1.3. Observed instantaneous cloud longwave radiative forcing

Figure 3 displays the outgoing fluxes (thus including cloudy areas) versus the clear-sky fluxes. It includes 29704 T106 grid boxes over which all ERBE measurements within 6 hours of 85/04/21 12GMT have been retained. All ERBE pixels located within a given T106 grid box are averaged. The cloud longwave forcing is shown as the vertical distance between a dot and the line of slope 1. The total CLF for that time is 36.2 W m^{-2}. In the tropical regions, characterized by high clear-sky longwave fluxes (generally over 270 W m^{-2}), CLF larger than 120 W m^{-2} are easily found, with CLF as high as 200 W m^{-2} seen in convective regions corresponding to outgoing fluxes as low as 80 W m^{-2}, indicating unity emissivity cloud tops at tropopause temperature (about 195 K).

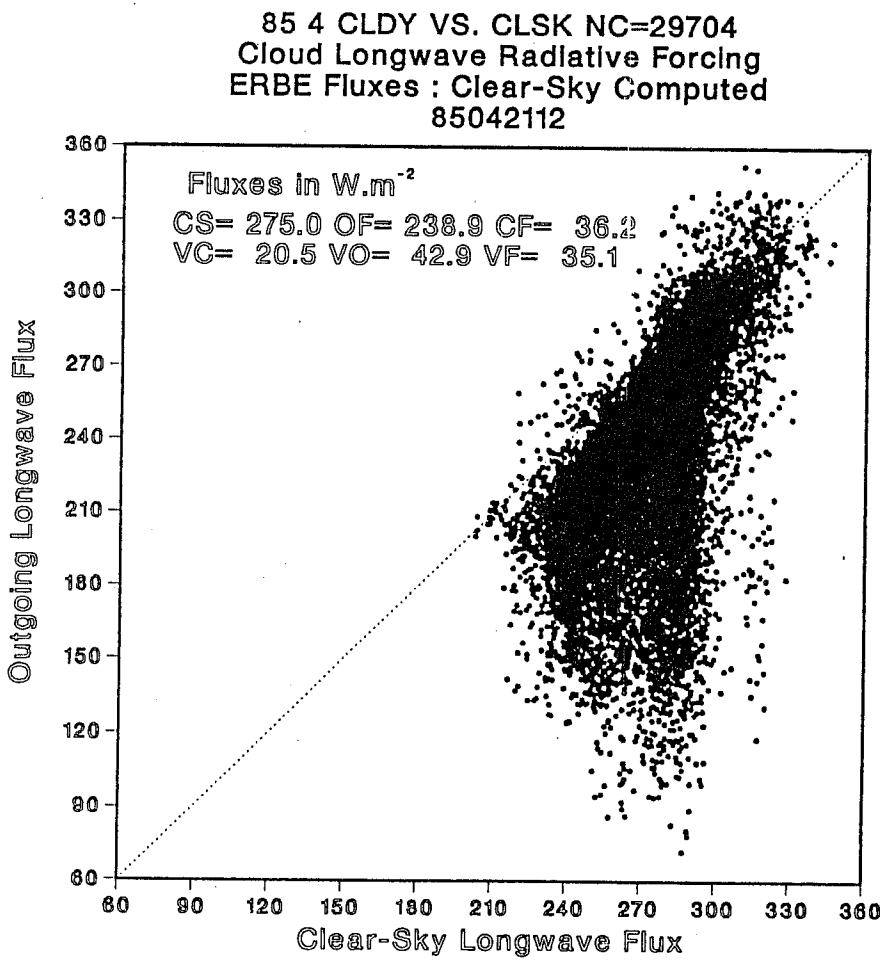

Figure 3: Computed clear-sky and observed outgoing fluxes in the 29704 T106 model grid boxes filled by ERBE data within ± 6 hours of 12GMT, on 21/04/85. Clear-sky fluxes are computed from analyzed T and q fields for 21/04/85, 12GMT.

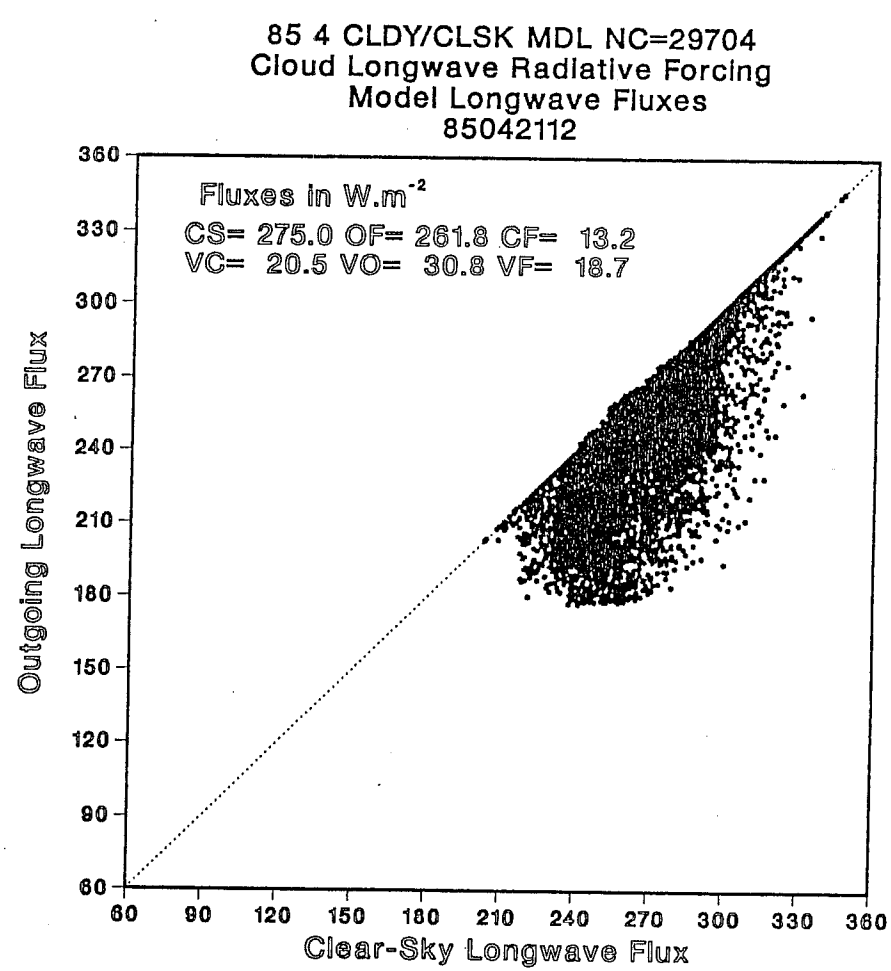

Figure 4: Model computed clear-sky and outgoing longwave fluxes in the 29704 T106 grid boxes of Fig. 3. Fluxes correspond to a 24 h forecast starting on 20/04/85, 12GMT using the operational cloud cover and diagnostic formulation of the cloud liquid water content.

1.4. Cloud longwave radiative forcing in the ECMWF model

It is interesting to look at how the ECMWF clouds behave in that respect, or more precisely, as we are not using the operational radiation code and embedded model cloud, whether or not the liquid water content diagnosed for the clouds and the related cloud radiative properties agree with the observations. Using the U. of Lille radiation code, shown to give reasonable estimates of the clear-sky fluxes (see section 1.2), we computed the outgoing longwave fluxes corresponding to the cloud distribution diagnosed by the model (Slingo, 1987). When comparing the operational cloud cover to observations, we usually get a fair agreement over mid-latitude areas where clouds associated with frontal systems prevail. Clouds of convective origin are well represented in the ITCZ.

Figure 4 presents the CLF derived from computed clear-sky and outgoing fluxes using the operational cloud cover and diagnostic formulation of the cloud liquid water content. This relates the LWC to the saturated water vapor mixing ratio of the layer where a cloud is present, with a proportionality factor $\gamma = 0.01$. The radiation scheme includes cloud optical properties following Stephens (1978) with the longwave emissivity varying as a function of the LWP.

Comparing Figures 3 and 4 shows that the model clouds have a much too small longwave radiative impact. The mean calculated outgoing flux is 261 W m^{-2} compared to the observed 238.9 W m^{-2}. The mean model CLF is about three times smaller than the mean observed CLF (13.2 W m^{-2} vs. 36.2 W m^{-2}). The largest CLF is about 100 W m^{-2} (and that is not the operational radiation scheme which is strongly negatively biased in clear-sky tropical atmosphere, thus giving about 260 W m^{-2} instead of 275 W m^{-2} for the clear-sky longwave flux, and therefore decreasing further the CLF in the operational model). The bias occurs for all values of the clear-sky flux, but clouds corresponding to warm surface temperatures (convective clouds over the tropics) have a particularly strong bias (70 W m^{-2} instead of 140 W m^{-2}). That bias is directly related to the small emissivity (around 0.1) that higher model clouds are given by the present diagnostic formulation via the small liquid water content. Measurements of emissivity of high clouds give higher values: 0.28 for a 1 km deep large scale jet-stream cirrus system (Platt, 1975) 0.65 for a 2 km deep anvils emanating from tropical thunderstorms (Platt et al., 1984), 0.70 for 2 km deep large cirrostratus systems (Platt and Dilley,

1979), 1.0 for tropical cirrus clouds overlying convective areas (Griffith et al., 1980).

The cloud cover diagnosed by the present cloud scheme can also be questioned: convective cloud cover is determined from the scaled time-averaged precipitation rate from the model's convection scheme with an upper limit of 80 percent. However, this 80 percent cloud cover may be attained only at the base height of the convective cloud as a further scaling by 0.25 is applied on convective cloud cover at all other levels to the top of the convective column, giving a maximum convective cloud cover of 20 percent in the higher layers (Slingo, 1987). It is quite clear that the combination of too transparent clouds and of underestimated convective cloud cover are responsible for the strong underestimation of the cloud longwave forcing in the ECMWF model.

2. COMPARISONS OF MODEL RADIANCES WITH ISCCP OBSERVATIONS

Whatever the uncertainties in an observed cloud climatology, the observed diurnal and seasonal variability of cloudiness are very strong signals which stand out above these uncertainties, and any cloud forecasting model, to be said successful, should be able to reproduce these signals with good fidelity. Although the seasonal cycle is certainly a very important signal to reproduce, the validation of the diurnal cycle is more directly relevant and easier to be carried out for a medium-range forecast model, such as the ECMWF operational model. The direct observed coupling between convective activity and cloudiness is needed to properly simulate the role of cloudiness in regulating the hydrological cycle.

For such a validation of the diurnal cycle, the only satellite data available at present with adequate time sampling come from geostationary satellites. The observational data used in this study are METEOSAT longwave window channel measurements compiled for July 1983 in the so called B3/CX format of the International Satellite Cloud Climatology Project (ISCCP; Schiffer and Rossow,1983, 1985). A full description of the ISCCP reduced resolution global radiance data set is given in WMO-ICSU (1985), with details on the navigation, calibration, and time and space sampling data processing.

For our study, we have used these data over the area 67.5 ^{o}N- 67.5 ^{o}S, 67.5 ^{o}W-67.5 ^{o}E, corresponding roughly to the field of view of METEOSAT. The calibrated radiance or equivalent brightness temperature T_B in the 10.5 -

12.5 μm channel is given every three hours (at 0000, 0300, ... 2100 GMT) with a horizontal resolution of 35 km at the subsatellite point (0 °N - 0 °W).

In order to have similar spatial resolution for both satellite observations and model outputs, the observed T_B are degraded to the T106 resolution of the current ECMWF forecast model. To be consistent, the comparison between satellite measured and model derived T_B's should be carried out over the same spatial scales. We have kept the comparison straightforward by simply averaging the satellite data over the $(1.125 \text{ deg})^2$ collocation grid, over which physical tendencies are calculated: we have thus averaged the T_B's of all ISCCP-B3 pixels whose center falls within a ECMWF model grid (typically such a grid contains between 4 and 15 pixels depending on the satellite viewing angle). Thus at the resolution of $(1.125 \text{ deg})^2$, we associate the mean observed T_B with that computed from the temperature, humidity and cloudiness profiles generated by the model.

The current operational analysis (as of december 1986) has been rerun for the period between 1 July and 10 July 1983, and a number of 5-day and 10-day forecasts have been produced from these analyses. Results presented in the following sections correspond to a forecast starting on 3 July 1983 at 12 GMT (83.07.03,12GMT), carried out with the version of the ECMWF model operational in Summer 1988 (cycle 30 of the libraries), and most comparisons between satellite observations and model outputs are shown for the period 83.07.04,00GMT - 83.07.08,00GMT.

Model outputs, simultaneous with the satellite observations, are produced every 3 hours, corresponding to the interval between two full radiation calculations in the model. The first 12 hours of the forecast have not been used in the comparisons, as cloud fields generated during that period are not reliable due to the spin-up of the model humidity and to the absence of convective cloudiness during the first 3 hours of any model forecast, as the convective cloudiness is diagnosed from the convective precipitation produced by the deep convection scheme (Kuo-type parameterization, see Tiedtke et al., 1988) accumulated over the previous 3 hours (Slingo, 1987). From fields of temperature, humidity and cloudiness forecast by the model, the radiance in the longwave window channel of METEOSAT is simulated using a longwave radiation scheme modified to compute channel radiances in the METEOSAT geometry, i.e., using the viewing angles of observation. The radiance is then converted to brightness temperature taking into account the filter function of the METEOSAT longwave window channel as given in WMO-ICSU (1985).

Comparisons of observed and simulated brightness temperatures can be

carried out over the whole METEOSAT field of view. However, the instantaneous character of the comparison on a T106 grid basis leads to fuzzy pictures, even more fuzzy in the case of brightness temperature representative of a cloudy atmosphere as cloudiness is a more spatially variable parameter than temperature or humidity, the two main governing parameters of the clear-sky brightness temperature. We can somehow get rid of this problem by looking at T_B's over larger areas on a more statistical basis. Those areas have to be small enough in their extent to encompass a relatively homogeneous background surface and, if possible, weather regime characterized by a unique type of cloudiness. But they have to be large enough to include a statistically significant number of grid boxes.

Eight limited areas (10.125 x 10.125 deg^2, corresponding to 9 x 9 T106 grid boxes) were finally defined, over which we have concentrated our study. The geographical distribution of these limited areas is shown in Figure 5, whereas the characteristics are given in Table 1. These areas have been chosen from METEOSAT visible imagery (ESA, 1983) as representative of a number of well defined atmospheric situations, where the signature of the cloudiness or/and of the surface on the brightness temperature is expected to be clear. They include three continental areas and five oceanic areas spanning the latitude range between 30^oN and 50^oS. Over these limited areas, the diurnal variations of the cloudiness and related brightness temperature as seen in the METEOSAT measurements and as produced in the model are studied using evolution histograms of the observed and simulated T_B's to assess the quality of the representation of the diurnal variations of the surface-atmosphere system by the ECMWF model.

Duvel and Kandel (1985) have illustrated the potential of the evolution histogram of the brightness temperature to study the diurnal variations of the surface-atmosphere system from satellite observations. In the evolution histogram of T_B, the x-axis represents the time evolution whereas the y-axis is the brightness temperature scale. Isolines define fractions of the total number of picture elements within each temperature class (taken as 1 K wide in our study). The warmer T_B then correspond to radiation coming from the surface and the colder to radiation emitted by the clouds.

Table 1: Characteristics of the eight limited areas.

N	Geographical location	Latitude	Longitude	Main features
1	Egypt, Lybia	29N-19N	20E-30E	clear-sky desert
2	Cape Verde Island	26N-16N	28W-18W	Stratiform clouds
3	Niger, Nigeria	20N-10N	5W- 5E	convection over land
4	Sierra Leone Basin	16N- 6N	34W-24W	convection over ocean
5	Central Africa	8N- 2S	21E-31E	convection over land
6	Off-coast Angola	7S-17S	0E-10E	Stratiform clouds
7	Central Mid-Atlantic	10S-20S	26W-16W	trade-wind Cu clouds
8	Gough Island	39S-49S	16W- 6W	S.H. frontal systems

We already noted the need for a comparison carried out over the same spatial scales, and for assessing the impact of the averaging processing performed on the observed T_B's. Figures 6 present the evolution histograms constructed from the observed T_B's either at the full ISCCP-B3 resolution or at the $(1.125\ ^\circ)^2$ resolution, for an area (n° 3 : The Niger-Nigeria area) where the distribution includes a wide range of T_B's from warm surface pixels to cold pixels related to convective cloud tops, thus where the impact of the averaging process is likely to be maximum. As seen in Figs. 6 ,the main features, relevant for validating a model parameterization are kept satisfactorily. The phase and amplitude of the diurnal cycle of the surface temperature and of the cloudiness are stable features in the averaging process, so that comparison with evolution histogram of the model generated T_B remains a meaningful exercise.

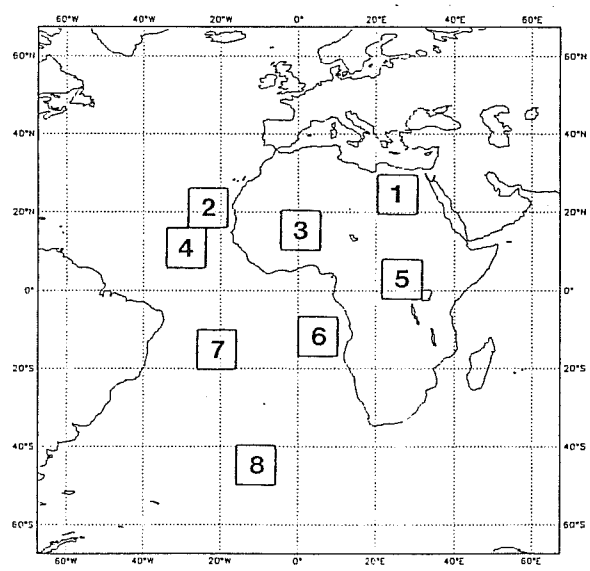

Figure 5: The location of the eight $(10.125\ \text{deg})^2$ limited areas over which the diurnal cycle of cloudiness and brightness temperature is studied.

Figures 6: The evolution histograms of the window brightness temperatures for the Niger-Nigeria. Left panel is the evolution histogram from full resolution ISCCP-B3 data; right panel is the evolution histogram from ISCCP data averaged over T106 grid boxes.

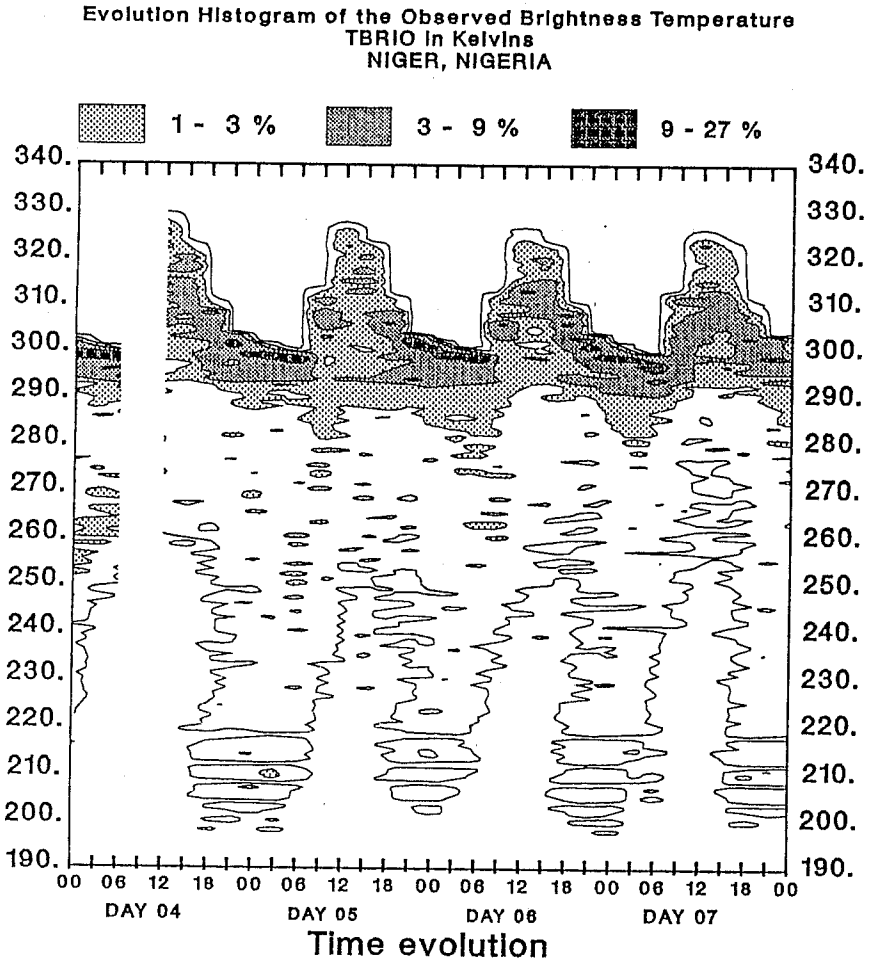

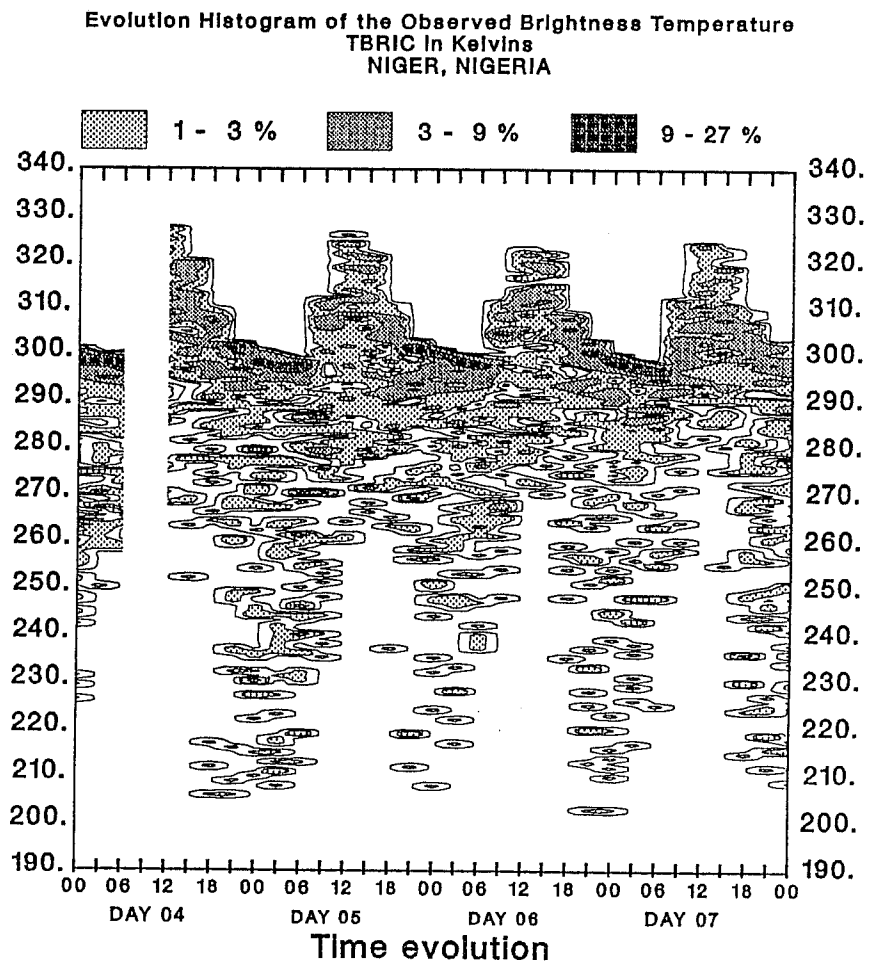

In Figures 7 to 14, we compare the evolution histograms of the METEOSAT longwave window channel T_B (hereafter EH (T_B)) over the eight limited areas. The right panels correspond to the ISCCP/B3 observations averaged over the T106 grid and the left panels correspond to the model-generated T_B's. Main difference in behaviour of observed EH (T_B) between oceanic and continental areas is obviously the weak or non-existing diurnal variation of sea surface temperature (Figs. 8, 10, 12, 13, 14) compared to the large variations of the surface temperature (5-30 K) appearing in the observed EH (T_B) in the land areas (Figs. 7, 9 and 11).

The areas over land correspond to different types of soil and vegetation which have been documented by Matthews (1983) and Wilson and Henderson-Sellers(1985). Desert barren soil prevails in area 1. This area displays a diurnal cycle of the CFD corresponding to mostly clear-sky conditions. Minimum surface T_B is found during the night (00 GMT), and maximum T_B occurs at 12 GMT. Interestingly enough, during daytime, the inhomogeneities in soil properties and thus in surface temperature give a spread of 10 K or more in the observed T_B's. The other two land areas present EH (T_B) showing the presence of cloudiness. Grassland with sparce shrub cover dominates and over the semi-desert area 3. Area 5 is covered by grassland with a small woody tree cover. Comparisons of Figs. 7, 9 and 11 show that the denser the vegetation, the smaller the T_B's and the narrower the range of diurnal variation of the warmest T_B's.

The five other areas are located over the ocean, with different types of cloudiness resulting from their latitude and prevailing circulation regime. Areas 2 (Cape Verde Island) and 6 (off-coast Angola) are located within zones of persistent stratiform clouds formed by subsidence above cold oceanic currents along the subtropical western side of the African continent. The presence of stratiform clouds shows up in the location of the maximum of the distribution of T_B's in the cold side of the EH (T_B) (at about 283-285 K in area 6). Presence of a clear-sky fraction over an otherwise cloudy oceanic area would rather give a marked narrow band on the warmer side (as in Figs. 10 and 13). In area 2, the low stratiform clouds display a marked diurnal cycle. The low-level cloud layer is thicker during the night (with a somewhat high top level at cooler temperature giving a smaller T_B). In response to the diurnal cycle of insolation, it becomes thinner and lower during daytime, giving larger T_B. Area 4, located in the oceanic ITCZ, displays an observed EH (T_B) characteristic of quasi-permanent convective activity with no marked diurnal cycle. Area 7 (Central mid-Atlantic) in the

Figures 7: The evolution histograms of the window brightness temperatures for the Egypt-Libya area. Left panel is the evolution histogram from ISCCP/B3 data averaged over T106 grid boxes; right panel is the evolution histogram produced by window brightness temperatures simulated from T, q and cloud fields forecast by the ECMWF model.

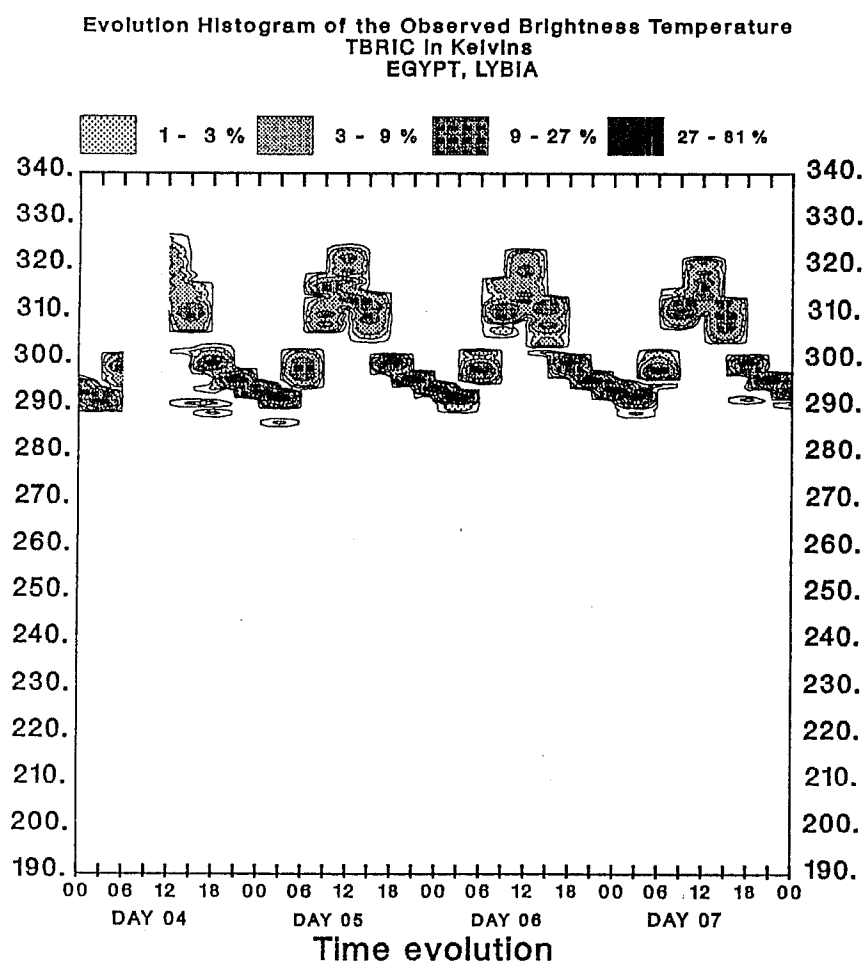

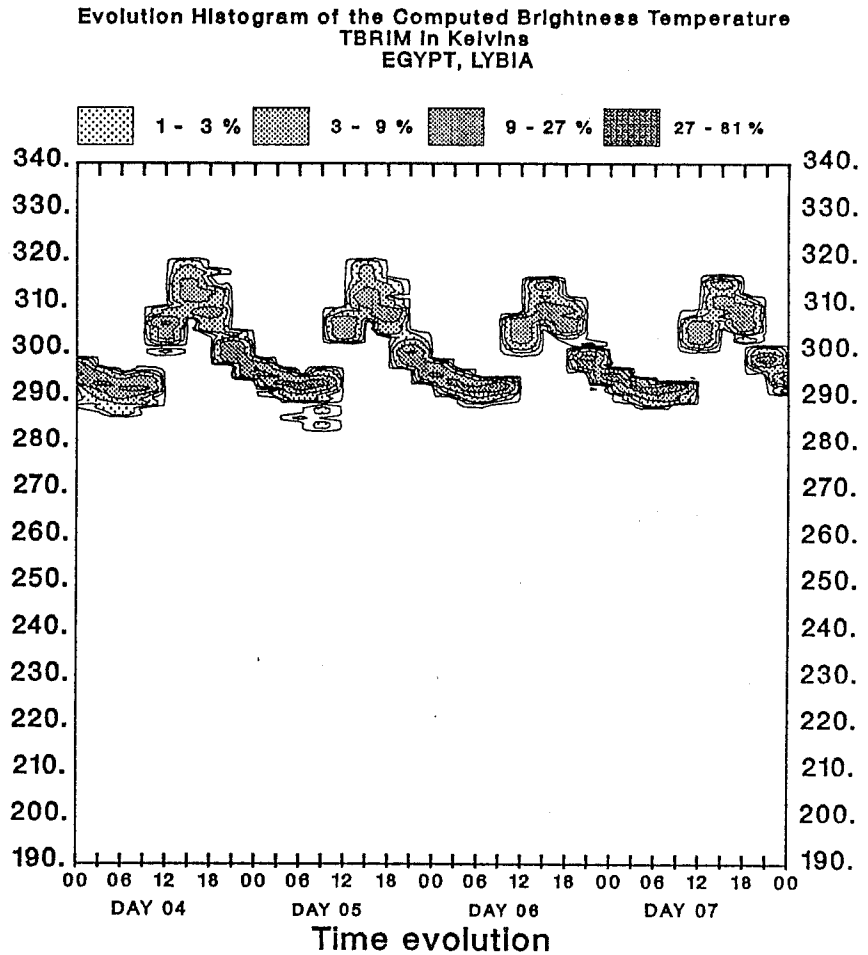

Figures 8: As in Figs. 7, but for the Cape Verde Island area.

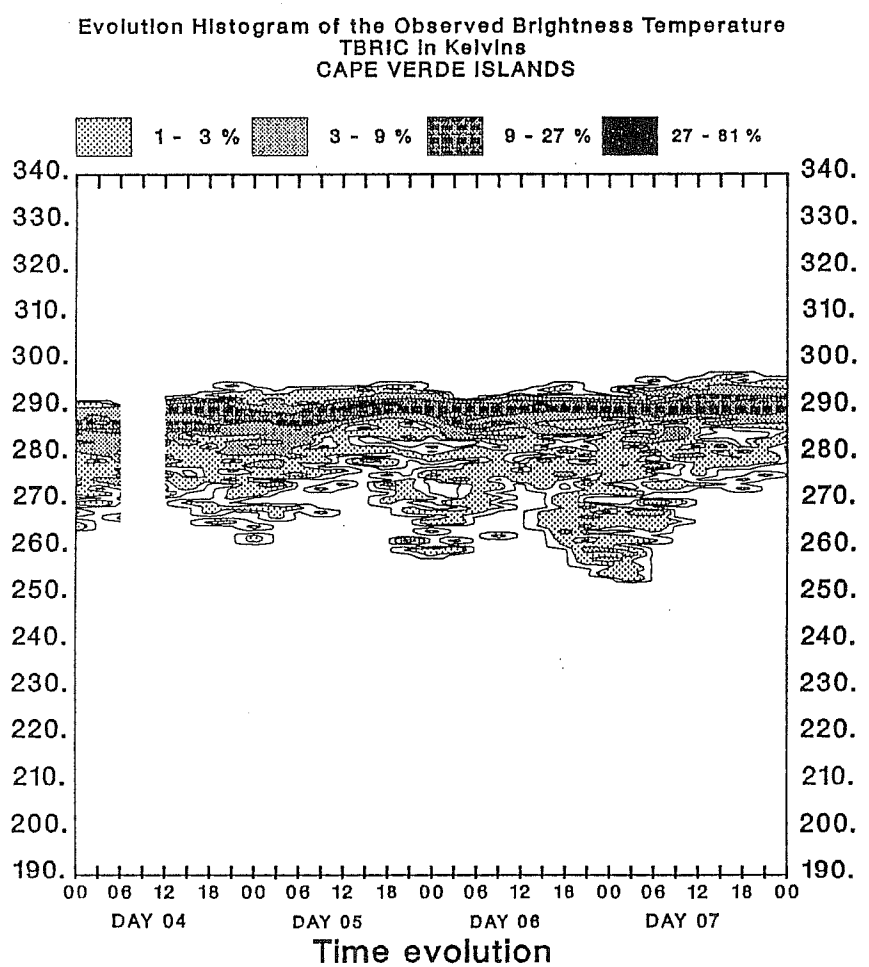

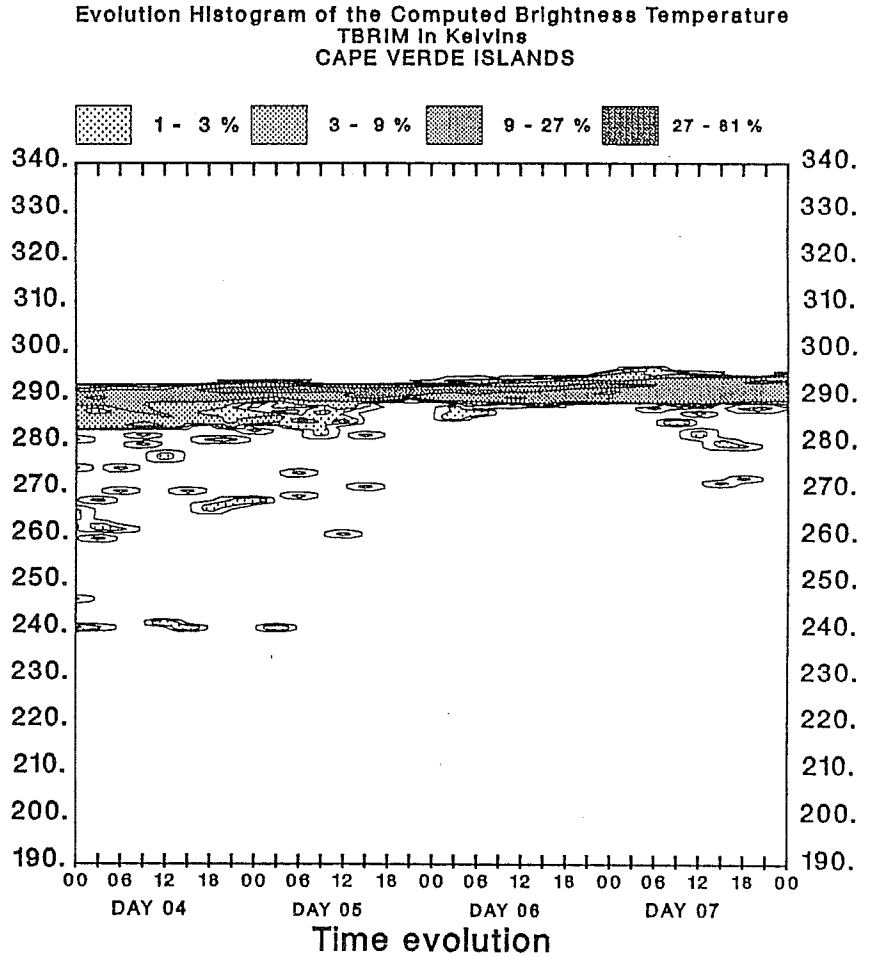

Figures 9: As in Figs. 7, but for the Niger-Nigeria area.

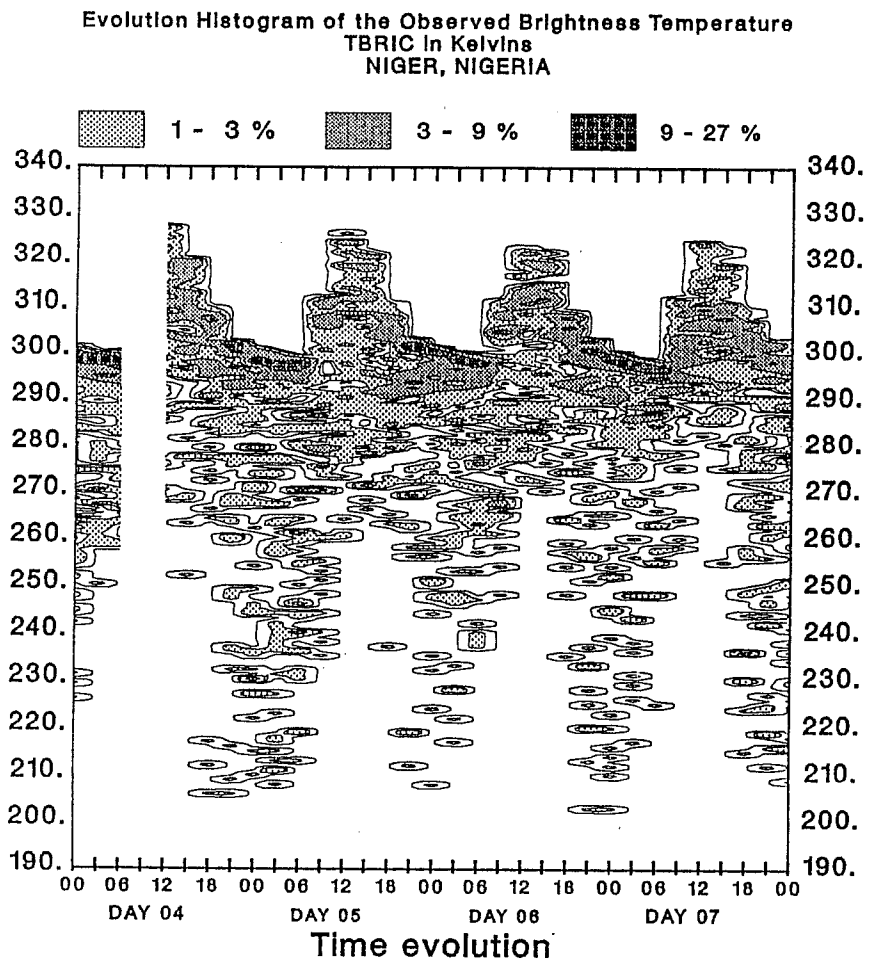

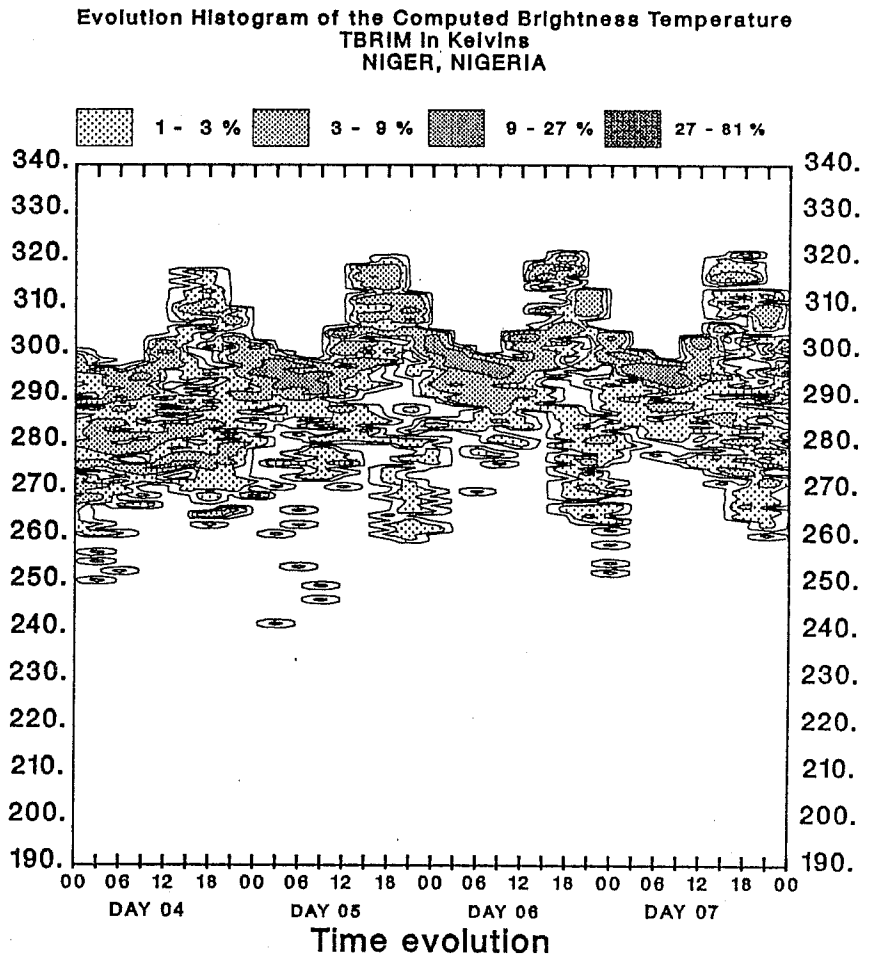

trade-wind region of the Southern hemisphere includes cumuliform clouds. A comparison of Figs. 12 and 13 corresponding to areas at similar latitudes shows how the small trade-wind cumulus clouds. The maximum of the observed EH (T_B) corresponds to the sea-surface T_B's and the sub-grid scale cumulus clouds show up as an extension of the observed histogram on the cold side (Note the difference with extended stratiform clouds at similar latitudes over area 6). Area 8 is located in the storm tracks of the Southern hemisphere. Frontal cloud systems are passing through these areas during the period study, giving a mostly cloudy to overcast sky. No particular diurnal cycle can be seen, but the observed EH (T_B) show an large cover of optically thick high-level clouds.

Comparison of observed and model-generated EH (T_B) allows to pinpoint various deficiencies in the representation of surface-cloud-radiation interactions in this version of the ECMWF model. For example, in area 1 (Figs.7) the model diurnal cycle of surface temperature is smaller than the observed one by about 5 K as the maximum model T_B is 320 K compared to the observed 325 K around 15 GMT. In such clear-sky dry conditions, this defect might be related to an inappropriate surface resistance for the transfer of heat. Similar features are seen over the other two land areas although the model is successful at diminishing the amplitude of the diurnal cycle of the surface temperature when the vegetation cover increases.

As already discussed by Slingo (1987), the cloudiness present over the sub-tropical oceans offers a challenge to the modeller. The extended stratiform clouds of the Eastern façade of the continents are vertically sub-grid scale whereas the trade-wind cumuliform clouds are horizontally sub-grid scale. As seen in Figs. 8, 12 and 13, the present ECMWF model does not produce any reasonable representation of these clouds. Where high cloudiness prevails in the observations (Figs. 9, 10, 11 and 14), the longwave radiative impact of the cloudiness is clearly underestimated. This can be explained by either a too small, a too low or a too transparent cloud cover. The comparison of EH (T_B) over Gough Island (area 8; Figs. 14), where the model is known to be quite successful at diagnosing the frontal clouds from relative humidity (Slingo, 1987), corroborates the findings of section 1.4, namely the presence of too transparent high clouds. Over land this problem gets worse as convective clouds are assigned too small a maximum cloud fraction (20 percent). However the model produces a correct phase for the diurnal cycle of the convective cloudiness over land. Over the convective

Figures 10: As in Figs. 7, but for the Sierra Leone Basin area.

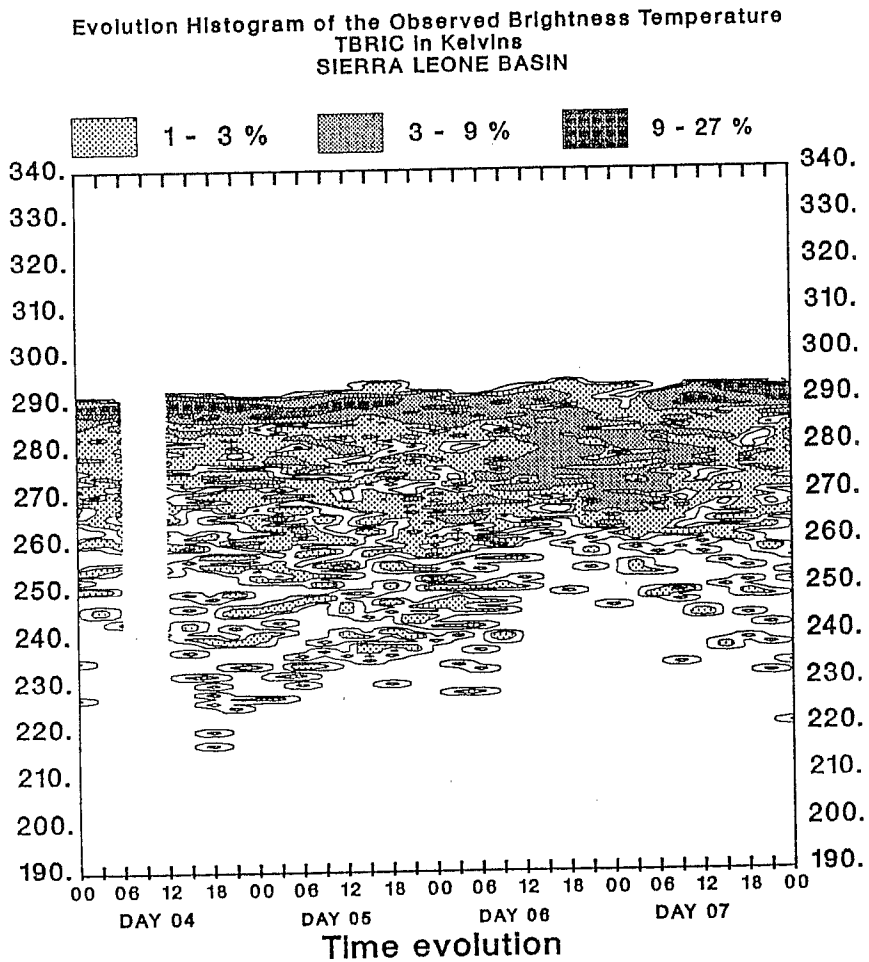

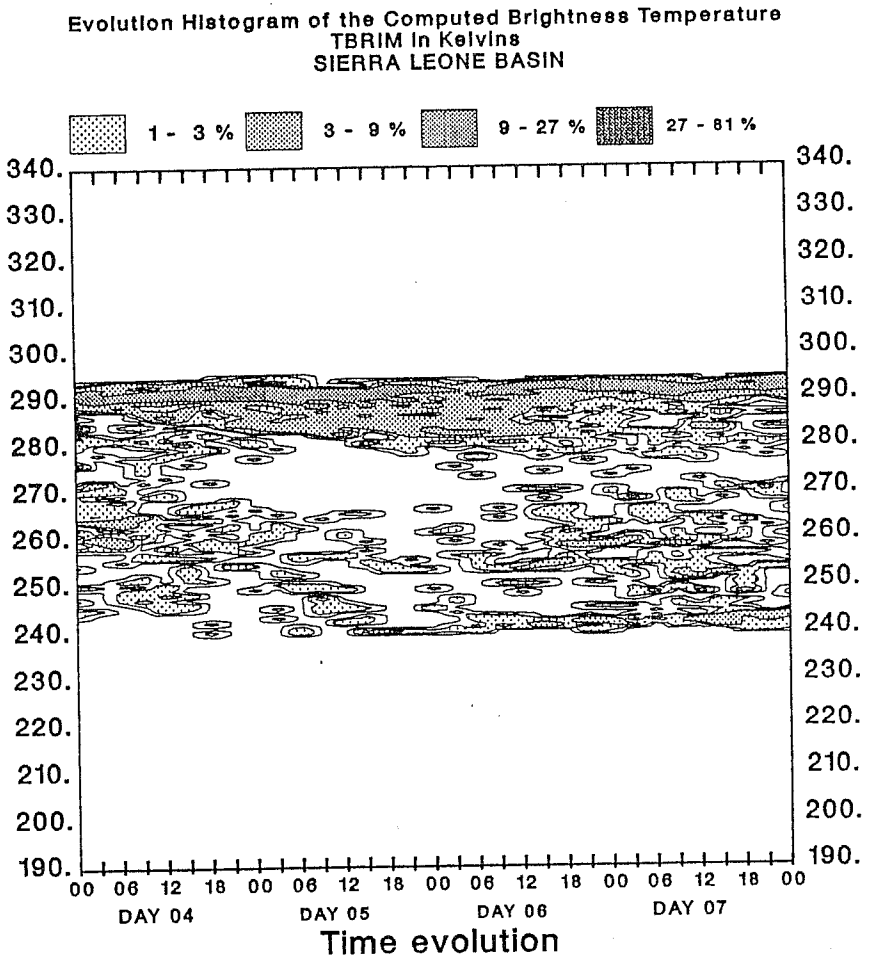

Figures 11: As in Figs. 7, but for the Central Africa area.

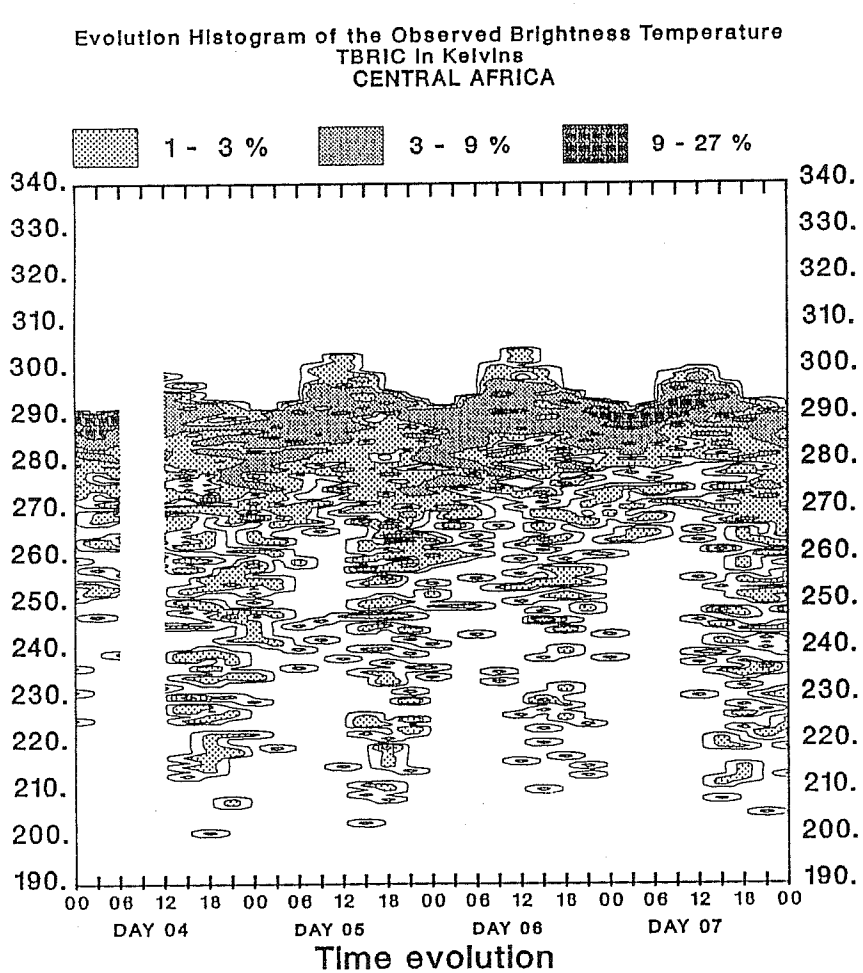

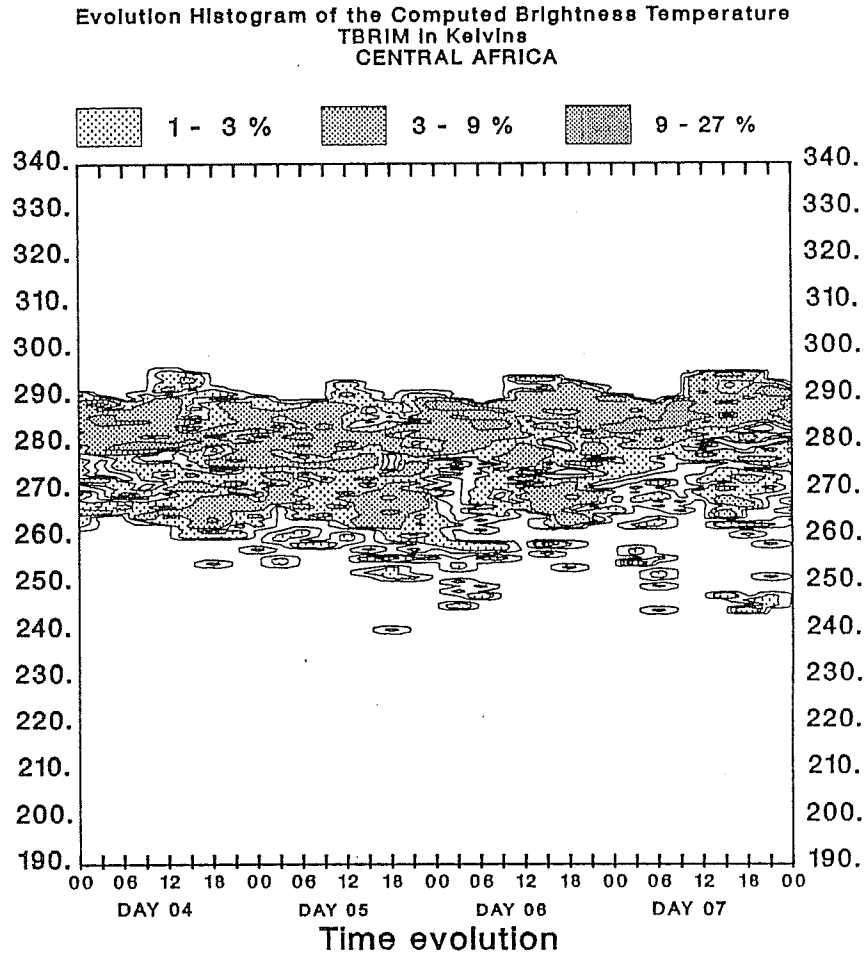

Figures 12: As in Figs. 7, but for the Off-Coast Angola area.

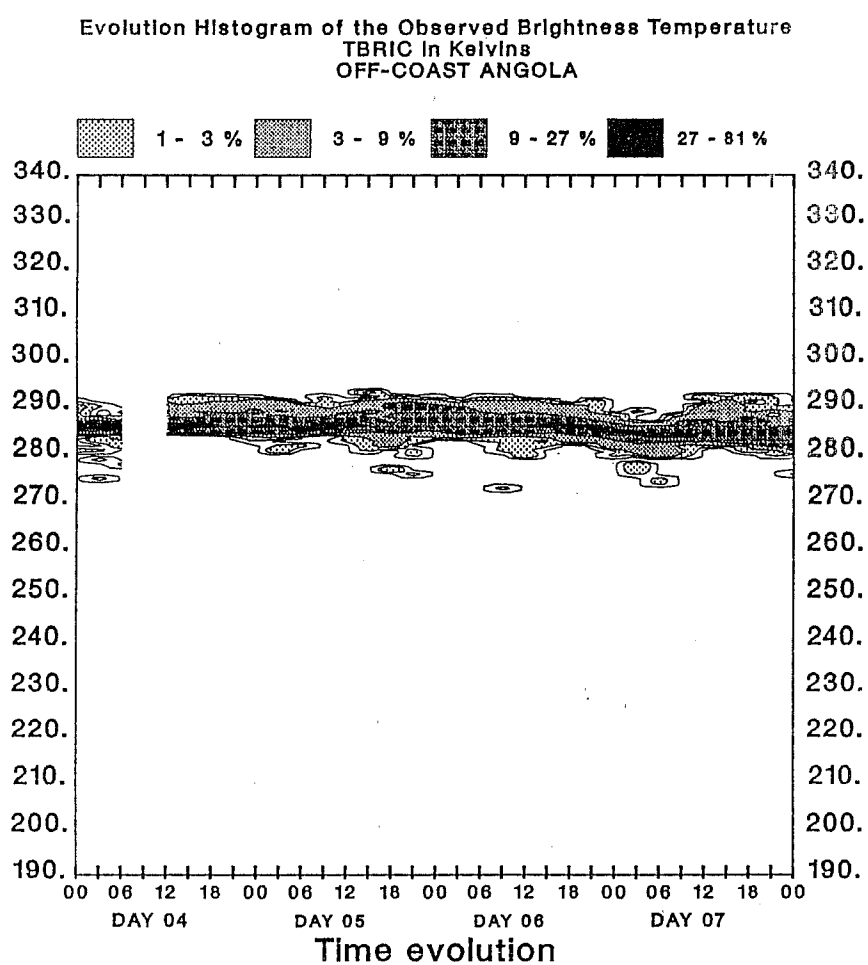

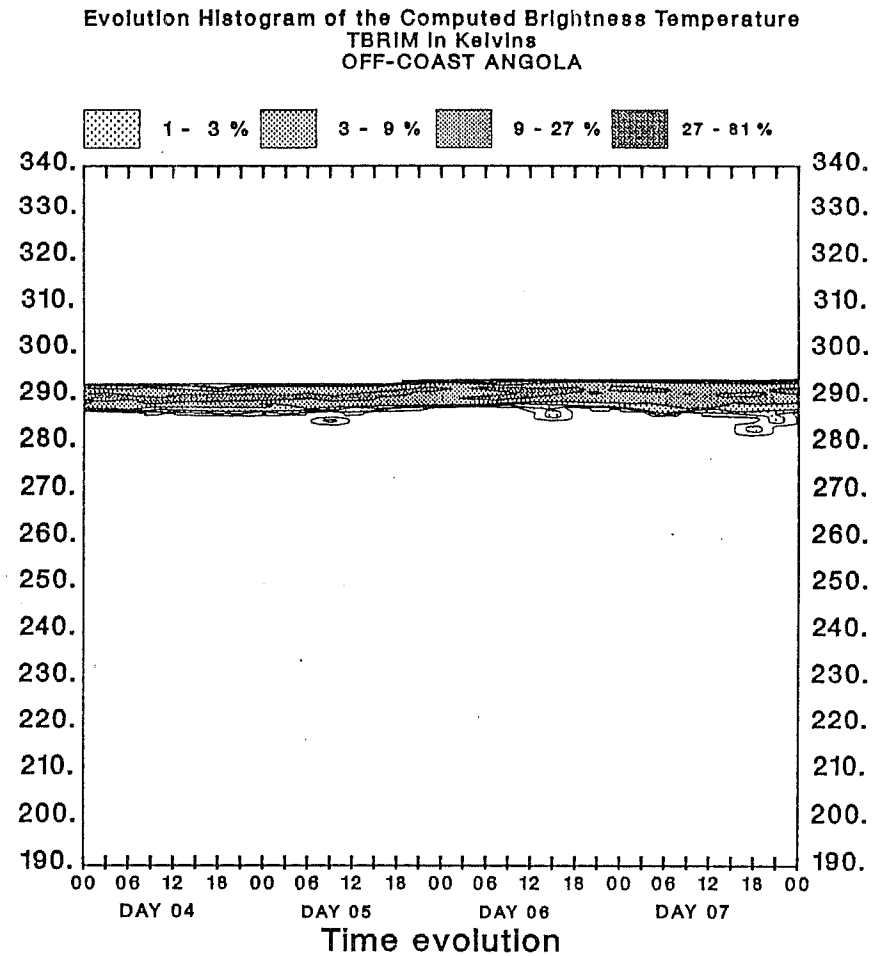

Figures 13: As in Figs. 7, but for the Central Mid-Atlantic area.

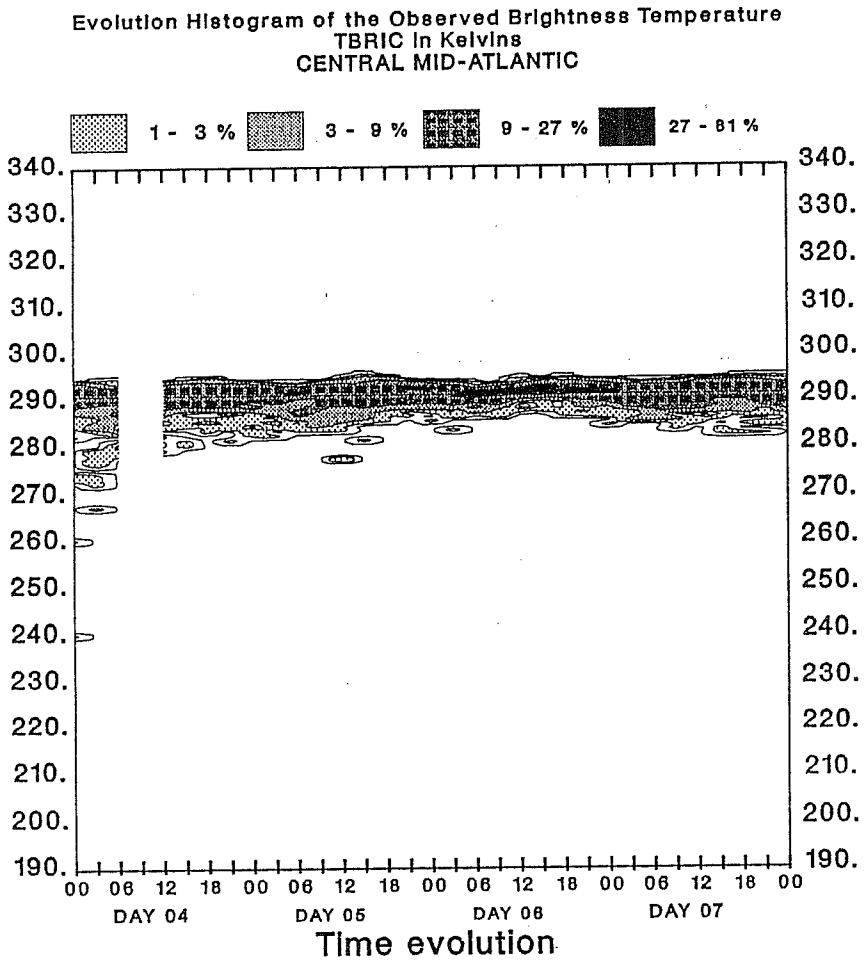

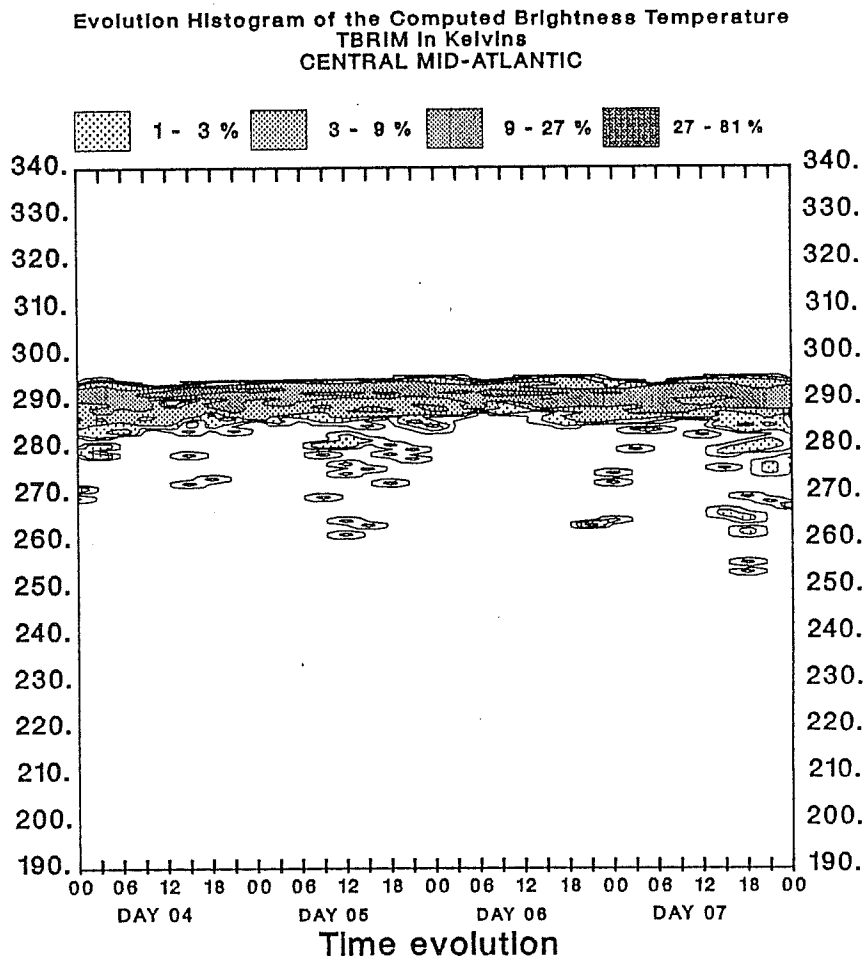

Figures 14: As in Figs. 7, but for the Gough Island area.

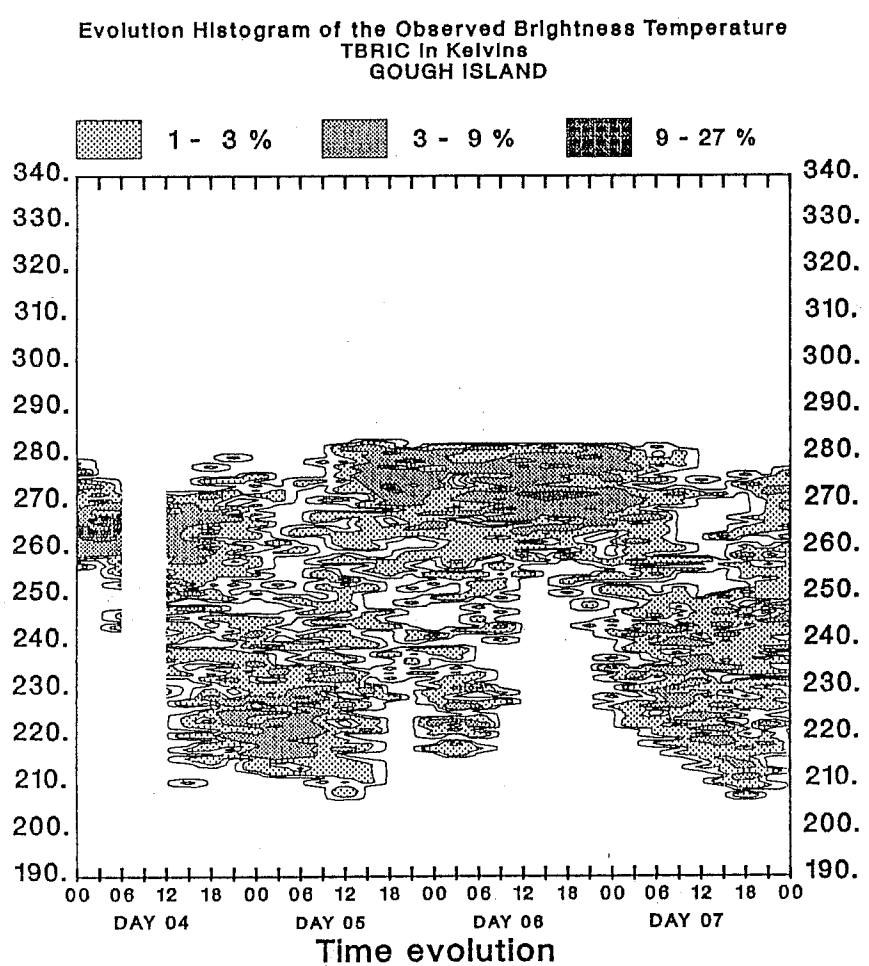

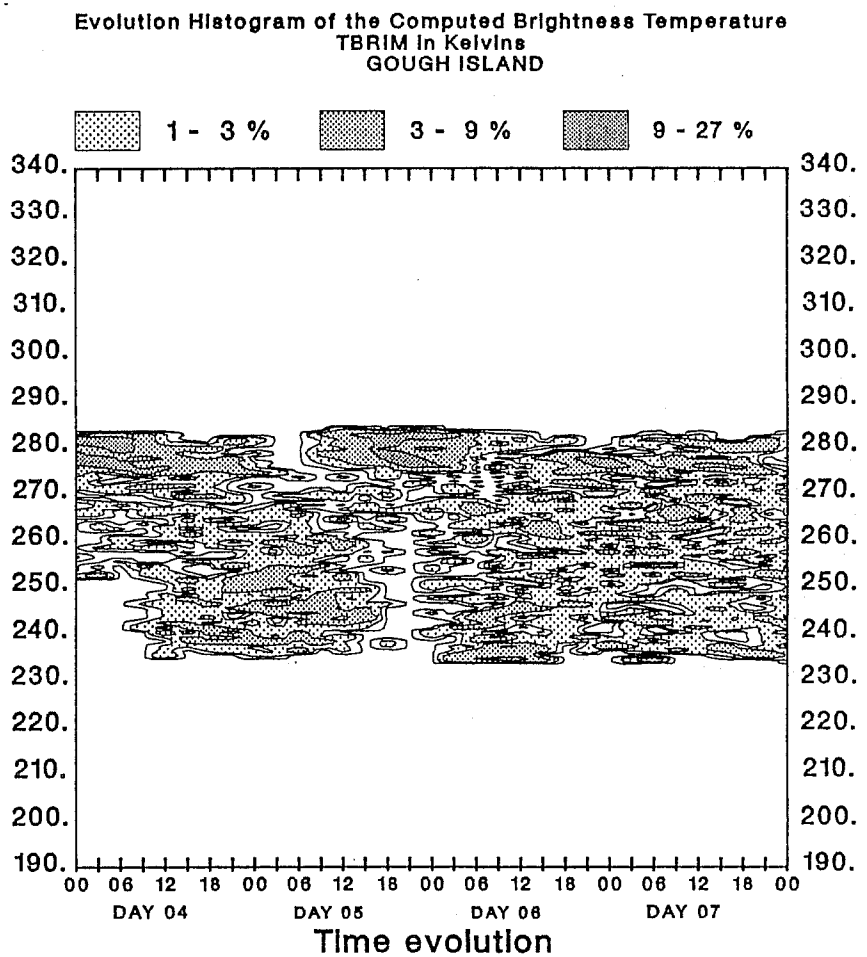

oceanic area, the model produces too few medium-level clouds as shown in Figs. 10.

3. FINAL REMARKS

This study is an attempt at assessing some aspects of the surface-cloud-radiation interaction parameterization in the ECMWF model, aiming first at validating the cloud prediction scheme use to derive several cloud properties (fractional cover, height, LWC) from the model's current atmospheric state, second at validating the cloud radiative scheme used to derive the radiation flux from some of these cloud properties, third at verifying the response of the model cloudiness to the diurnal forcing of insolation.

The approach used in this paper has followed recommendations by ECMWF (1984) and proposals by Slingo (1987), namely to produce model quantities directly comparable to satellite measurements.

The objective of this study has been a "validation" to signify that its main purpose has been to provide error estimates: improvement of the various parameterization schemes appearing in this study requires more difficult iterative studies of model testing and data comparison, clearly out of scope of this paper.

The radiation code used to produce the extra radiation diagnostics of this study has now become the operational ECMWF radiation scheme. The impact of the radiation scheme fully interactive with the rest of the ECMWF model will be reported elsewhere.

A similar study comparing observed and model-generated shortwave radiances would be very interesting. However, it is hindered with more difficult problems related to the bi-directional reflectance properties of the surface, a surface albedo fixed at mean annual value in the ECMWF model, the shortwave radiances being more sensitive to the details of the cloud microphysics (compared to bulk mass absorption coefficients in the longwave).

Acknowledgments: Yves Fouquart helped me a lot during the very frustrating first stages of this study, namely in allowing the ERBE and ISCCP tapes to be read by the ECMWF computer system and in the construction of the match-ups dataset.

REFERENCES

Barkström, B.R., 1984: The Earth Radiation Budget Experiment (ERBE). Bull. Amer. Meteorol. Soc., 65, 1170-1185.

Barkström, B.R., and G.L. Smith, 1986: The Earth Radiation Budget Experiment: Science and Implementation. Rev. Geophys., 24, 379-390.

Duvel, J.-P., and R.S. Kandel, 1985: Regional-scale diurnal variations of outgoing infrared radiation observed by METEOSAT. J. Clim. Appl. Meteor., 24, 335-349.

ECMWF, 1984: Workshop on Cloud Cover Parameterization in Numerical Models. ECMWF, Reading, U.K., 26-28 November 1984.

ESA, 1983: METEOSAT Image Bulletin: July 1983. MDMD/Data Service, European Space Agency Scientific and Technical Public. Branch, ESTEC, Noordwijk, The Netherlands, 62 pp.

Griffith, K., S.K. Cox, and R.G. Knollenberg, 1980: Infrared properties of tropical cirrus clouds inferred from aircraft measurements. J. Atmos. Sci.,37, 1077-1087.

Hartmann, D.L., and E.E. Recker, 1986: Diurnal variation of outgoing longwave radiation in the tropics. J. Clim. Appl. Meteor., 25, 800-812.

Hartmann, D.L., V. Ramanathan, A. Berroir, and G.E. Hunt, 1986: Earth radiation budget data and climate research. Rev. Geophys., 24, 439-468.

Matthews, E., 1983: Global vegetation and land use: new high-resolution databases for climate studies. J. Clim. Appl. Meteor., 22, 474- .

McClatchey, R.A., R.W. Fenn, J.E.A. Selby, F.E. Volz, and J.S. Garing, 1972: Optical properties of the atmosphere, 3rd ed., AFCRL-TR-72-0497, Environment Research Paper 411, Bedford, Mass., 108 pp.

Morcrette, J.-J., 1989: Radiation and cloud radiative properties in the ECMWF operational weather forecast model. J. Geophys. Res., accepted for publication.

Morcrette, J.-J., and Y. Fouquart, 1985: On systematic errors in parametrized calculations of longwave radiation transfer. Quart. J. Roy. Meteor. Soc., 111, 691-708.

Morcrette, J.-J., and J.-F. Geleyn, 1985: On the influence of different radiation parameterizations on model-generated radiation fields. Quart.J.Roy.Meteor.Soc., 111, 565-585.

Morcrette, J.-J., L. Smith, and Y. Fouquart, 1986: Pressure and temperature dependence of the absorption in longwave radiation parameterizations. Beitr. Phys. Atmosph., 59, 455-469.

Platt, C.M.R., 1975: Infrared emissivity of cirrus. Simultaneous satellite, lidar and radiometric observations. Quart. J. Roy. Meteor. Soc., 101, 119-126

Platt, C.M.R. and A.C. Dilley, 1979: Remote sounding of high clouds: II. Emissivity of cirrostratus. J. Appl. Meteor., 18, 1144-1150.

Platt, C.M.R., A.C. Dilley, J.C. Scott, I.J. Barton, and G.L. Stephens, 1984: Remote sounding of high clouds. V: Infrared properties and structures of tropical thunderstorm anvils. J. Climate Appl. Meteor., 23, 1296-1308.

Ramanathan, V., 1987: The role of earth radiation budget studies in climate and general circulation research. J. Geophys. Res., 92, 4075-4095.

Reed, R.J., and K.D. Jaffe, 1981: Diurnal variation of summer convection over West Africa and the tropical eastern Atlantic during 1974 and 1978. Mon. Wea.Rev., 109, 2527-2534.

Schiffer, R.A., and W.B. Rossow, 1983: The International Satellite Cloud Climatology Project (ISCCP): The first project of the world climate research programme. Bull.Amer.Meteor.Soc., 76, 779-784.

Schiffer, R.A., and W.B. Rossow, 1985: ISCCP Global Radiance Data Set: A new resource for climate research. Bull.Amer.Meteor.Soc., 66, 1498-1505.

Slingo, J.M., 1987: The development and verification of a cloud prediction scheme for the ECMWF model. Quart. J. Roy. Meteor. Soc., 113, 899-928.

Slingo, A., and J.M. Slingo, 1988: The response of a general circulation model to cloud longwave radiative forcing: I. Introduction and initial experiments. Quart. J. Roy. Meteor. Soc., 114, 1027-1062.

Stephens, G.L., 1978: Radiative properties of extended water clouds. Parts I and II., J. Atmos. Sci., 35, 2111-2132.

Tiedtke, M., W.A. Heckley, and J. Slingo, 1988: Tropical forecasts at ECMWF: On the influence of physical parameterization on the mean structure of forecasts and analyses. Quart. J. Roy. Meteor. Soc., 114, 639-664.

WMO-ICSU, 1985: International Satellite Cloud Climatology Project (ISCCP): Description of reduced resolution radiance data. WMO/TD-No. 58, Geneva, Switzerland.